Response of high-altitude clouds to the galactic cosmic ray cycles in tropical regions

Hiroko Miyahara[1,2,*], Kanya Kusano[3], Ryuho Kataoka[2,4,5], and Emile Touber[2,6]

[1]Humanities and Sciences/Museum Careers, Musashino Art University, Tokyo, Japan.

[2]Okinawa Institute of Science and Technology, Okinawa, Japan.

[3]Institute for Space-Earth Environmental Research, Nagoya University, Aichi, Japan.

[4]National Institute of Polar Research, Tachikawa, Japan.

[5]SOKENDAI, The Graduate University for Advanced Studies, Kanagawa, Japan.

[6]Department of Mechanical Engineering, Imperial College London, London, England

*Corresponding author: Hiroko Miyahara (miyahara@musabi.ac.jp)

Abstract

Galactic cosmic rays (GCRs) are one of the possible mediators of the solar

influence on climate. However, the impacts of GCR on clouds and climate systems are not fully understood. In this paper, we show that the high-altitude clouds associated with deep convective activities are responding to the decadal-scale cycles of GCRs and that the susceptible areas are seasonally variable. Most notable responses were found in August over tropical land areas, suggesting that the susceptivity of clouds to GCRs depends on the depth of convective activities and the abundance of aerosol precursor materials. Furthermore, following the activation of high-altitude cloud formation, an increase in sea surface temperature (SST) gradient was observed over the Pacific. Although the response of SST to solar activity has mostly been discussed as mediated by solar radiations, we propose that another mechanism is possible: through the impact of GCRs on clouds and the resultant changes in atmospheric circulations.

Introduction

The possible responses of climate to solar activity variations have been reported for various time scales [1], and several mediating mechanisms have been proposed, including the effects of solar radiations [2–5] and GCRs modulated by

39 solar-wind magnetic field [6,7]. Notable responses of climate to solar activity have
40 been observed for millennial [8,9] and centennial time scales [10,11]; however,
41 identifying the relative importance of mediating solar-activity related parameters
42 is difficult at such time scales, as the radiative and magnetic outputs of the Sun
43 vary in complete correspondence. To identify the contribution of each of the
44 parameters and trace the propagation of their impacts, it is needed to examine
45 the shorter time scales, such as those associated with the solar decadal cycle, or
46 even shorter, where the temporal variation of the solar radiative outputs and
47 GCRs are slightly different [12,13].

48 Solar radiations vary based on the emergence and disappearance of sunspots
49 and faculae on the solar surface [14]. Therefore, they change along with the
50 decadal-scale variation of the activity level of sunspots. However, the flux of
51 GCRs incident to the Earth's atmosphere is attenuated by the solar wind
52 magnetic field in the heliosphere and is thus dependent on the evolution of the
53 configuration and its direction [15]. As a result, the flux of GCRs is dependent on
54 the solar magnetic polarity that reverses every solar cycle maximum (see Fig S1).
55 In addition, the transient intensification of the magnetic fields associated with
56 solar coronal mass ejections contributes to the shielding of GCRs [16]. Due to the
57 travel time of the solar magnetic field in the heliosphere and its influence on the

58 trajectory of GCRs, the variation of GCRs at Earth occasionally delays up to ~1.4
59 years relative to the decadal variations in solar activity level [17,18]. Such
60 features might allow identifying the potential contribution of GCRs to the Sun–
61 Climate connection.

62 The possible impact of the decadal-scale solar activity cycle on climate has been
63 reported, e.g., in the North Atlantic region [19–21] and the tropical region [5,22–
64 24]. Recent studies have suggested that an increased solar activity results in a
65 reduction in the east-west gradient of SST over the Pacific and in a weakening of
66 the Pacific Walker Circulation [5]. These decadal-scale Sun-Climate connections
67 have been mostly attempted to be explained by the so-called “top-down”
68 mechanism, through which solar UV (SUV) influences stratospheric temperature
69 and subsequently alters tropospheric circulation [2,3] or by the “bottom-up”
70 mechanism, through which the total solar irradiance (TSI) warms up the ocean to
71 change atmospheric circulation [4,5]. However, significant positive feedback is
72 needed for the latter mechanism to explain the observed temperature variations,
73 as the variability of TSI over solar cycles is as small as 1 W/m^2.

74 It is, however, also possible that GCRs contribute to the decadal-scale Sun–
75 Climate connection through their impacts on clouds by the formation of aerosols
76 [7,25–27], by enhancing the collision efficiency between aerosols and cloud

droplets [28–30], or by stabilizing the molecular cluster to grow to cloud condensation nuclei [31–33]. However, it is not well understood how their effects might proceed in actual environments and how those impacts propagate in the climate system.

Originally, it was suggested that the cloud covers over oceans are enhanced with the increase in GCRs [6]. Later on, it was demonstrated that the low-altitude clouds over oceans are most significantly correlated to GCR variations [34]. However, both theoretical estimates and the laboratory chamber experiment have indicated that GCR-induced aerosol formations are rather efficient at low temperatures [26,35–37] (i.e., at high altitudes). The upper troposphere is also favorable in terms of the abundance of GCR-induced ions [38–40]. Deep convection is a possible method for supplying aerosol precursors from the biogenic activities at the ground or ocean surfaces to the upper troposphere [35,41]; therefore, the high-altitude clouds near highly convective areas are potentially most susceptive to GCRs, although the deep convection may also contribute to the transport of newly-formed cloud condensation nuclei to the lower troposphere to change the cloud properties [42].

The impact of GCRs through the formation of aerosols may only be emphasized if there are few preexisting aerosols in an ambient environment [43], as newly

formed aerosols tend to be adsorbed to preexisting aerosols if they are abundant. Atmospheric aerosols, including the ones that have anthropogenic origins, are mostly confined within ~4 km from the surface, except over the mountains with high elevations [44]. This factor also suggests a possibility that only the middle to upper troposphere meets the criteria of significantly being impacted by GCRs.

In this paper, we examine the response of high-altitude clouds based on records over the past 43 years. Due to the possible artifactual influence from satellite-based observations [45], it is vital to examine the cloud behaviors based on multiple independent data sets and to concentrate on the fluctuations except for long-term trends. Therefore, in this work, we base on two records (see methods) and focus on the response at the decadal scale. We used monthly-resolved high temporal-resolution data to constrain the possible conditions required for clouds so as to significantly respond to GCR variations.

Results

Relationship between high-altitude clouds and GCR cycles

The monthly data of high-altitude clouds, as monitored by Outgoing Longwave Radiation (OLR) and those of International Satellite Cloud Climatology Project

(ISCCP) H-series Gridded Monthly (HGM), were compared with GCR cycles (see Methods). Then, it was found that both series consistently indicate that there are regions in the tropics where high-altitude clouds show significant positive correlations to decadal-scale GCR cycles (Figs 1 and 2, also see Supplementary Figs S2–S3), suggesting that GCRs may be contributing to the changes in cloud activity. However, the areas were localized, and they significantly varied based on the seasons. Most significant correlations were found in August for the areas in which the formation of high-altitude clouds is active (see Fig 1), supporting the above-mentioned hypothesis; however, they were localized to the land areas and nearby oceans. There were also some regions in which high cloud formations were suppressed (see below). In boreal winter, the areas showing significant correlations were migrated to the convective regions in the southern hemisphere (Fig 2, also see Fig S3). The signals were weaker compared with those of August; however, a prompt response was observed around the northern tip of Australia and the northwest coast of South America (Fig 2a). Figures 1f–i and 2f–i indicate the OLR range that achieved the maximum correlation for each grid. While the threshold of 200 W/m^2 or lower suggests that the response is limited to the high-altitude clouds, the threshold of 230/m^2 or higher implies that the addition of mid- and possibly lower altitude clouds improves the correlation. For example, Figures

1f and 2f suggest that the correlations off the northwest coast of South America involve the response of mid-altitude clouds.

In August, the correlations were maximized in 1 year (Fig 1b) and diminished afterward (Fig 1c–d). Such lagged responses imply that a positive feedback mechanism exists behind the GCR–cloud connection. The correlations around the Indonesian maritime continent further delay (Fig 1c–d), suggesting an impact through the mechanism involving atmospheric and ocean coupling. Similarly, the signals around the northern tip of Australia and the northwest coast of South America in January diminished after 1 year, whereas the correlations around the Indonesian maritime continent were maximized in 2–3 years (Fig 2c–d).

The maximum variability of the existence ratio of high-altitude clouds over the GCR cycle is shown in Figures 1j and 2j. The obtained maps indicate that there are regions where the variability is much larger than expected from the ion production rate in the tropics (see Fig S12 of [37]), also supporting the existence of a positive feedback mechanism. For example, while the variability of ion production rate in the upper troposphere is up to ~20 % around 20-30°N and 20-30°S in the tropics and is smaller in the lower latitude regions, the variability of the fraction of days OLR is equal to or lower than 200 W/m^2 is larger than 20 % in August around eastern India and Bangladesh, where the mean fraction is

153 ~40 % (Fig 1e, also see Fig S4 for the time profile), although the corresponding
154 variability of cloud amount needs further investigations. Note that the
155 enhancement in the fraction of days with the presence of high clouds as
156 estimated based on the OLR thresholds may also be caused by the uplift of the
157 convective cloud system in addition to the increase of cloud amount itself.
158
159 **Relationship between SST and the GCR cycles**
160 Figure 3a–e indicates the correlation coefficient between SST and GCRs in
161 August when the most notable correlations were found for cloud activity. Figure
162 3f exhibits the spatial pattern of SST in August. The figures indicate that decadal-
163 scale forcing results in a characteristic spatial pattern in the central and western
164 Pacific. While the SST in the central Pacific tends to be cooled as GCR is
165 enhanced, especially in the winter hemisphere (Fig 3g), the SST in the
166 southwestern Pacific tends to be warmed, suggesting that the trade winds over
167 the Pacific region are intensified at the GCR cycle maxima. This tendency is
168 consistent with the previously suggested reduced east–west SST gradient and
169 the weaker trade winds at the solar cycle minima [5]. However, the response of
170 SST to TSI, which was suggested as the forcing parameter, delays by 1 year
171 compared to the case of GCR and was maximized with a lag of 3 years (see Fig

3h–n). The relationship between SST and SUV is more or less the same for TSI (see Fig S5) and is peaked with a lag of ~3 years.

The areas showing significant correlations between SST and GCRs with no time lag were limited to the southern edge of the tropical zone around 20–30°S 100–130°W (Fig 3a); however, the impacts were expanded and maximized with a lag of 2 years (Fig 3c). The maximum temperature change around the equatorial region over the GCR cycle was as large as 1.7 K and was observed at around 160°E–160°W (Fig 3g). Regarding January, the east–west contrast was less well structured. However, the maximum change around the region reached 2.1 K (see Fig S6). This region is often characterized by the El Niño modoki events [46] and has been examined using the Niño 4 index, one of the indices of the El Niño–Southern Oscillation. Although the Niño 4 index is derived based on the SST over the region wider than those indicating correlations to GCRs, and thus the correlation coefficient between Niño 4 and GCRs is relatively lower, the lead-lag analysis supports that the decadal component of SST in this region lags that of GCRs by about 2 years (see Fig S7a–b).

Figure 3c,g indicates that the areas showing correlation with GCRs include the Bering Sea, which is within the region characterized by the Pacific Decadal Oscillation [47], and that the correlations become maximum with a lag of 2 years.

The lead-lag analysis between the Pacific Decadal Oscillation index and the GCRs shows that the correlation becomes maximum when the lag is about 2–3 years (see Fig S7c–d), supporting that the decadal component of the Pacific Decadal Oscillation also lags that of GCRs.

In the cases the decadal components of the Niño 4 and the Pacific Decadal Oscillation indices were compared to the tropical high-altitude clouds, correlations were observed with a spatial pattern similar to those of Figure 1a–b; however, they were maximized when the lag was −2 to −1 years (see Figs S8 and S9), supporting that the decadal components in the Pacific Decadal Oscillation and the Niño 4 indices lag those of tropical cloud activities. Note that the direct comparison between the Niño 4 index and the Pacific Decadal Oscillation index shows that they are linked with an occasional lag of up to 1 year (see Fig S7e–f).

Relationship between the surface pressure, zonal/meridional winds, and GCR cycles

The comparison between the surface pressure and GCRs (Fig 4a–f) indicates increased pressure around the southern edge of the tropical zone in the Pacific (Fig 4a), and the impacts are further intensified and expanded toward the northern hemisphere in 1–2 years (Fig 4b–c). On the contrary, the tropical regions

between 120°W and 100°E indicate a tendency of decreasing pressure for the higher GCR, especially over the oceans. The zonal and meridional wind speed compared with GCRs suggests a possible intensification of trade winds or a westerly migration of the deep convection core around the western Pacific, especially in the northern hemisphere (see Fig S10). When the pressure data were compared with TSI, slightly different behaviors were recognized (Fig 4g–l). One is the absence of immediate response (Fig 4g), and the other is the 1-year delay in the signals (Fig 4h–j) compared with the case for GCR (Fig 4a–c).

Discussion

Although the impacts of solar cycles on climate have so far been mostly discussed under the framework of the “top-down” or “bottom-up” mechanisms described earlier, the present results suggest that another mechanism is possible: “deep-convective-clouds-mediated” mechanism through the influence of GCRs on the development of deep convective clouds, and their impact on atmospheric circulation and SST gradient.

The monthly-resolved high-resolution data allowed us to identify the areas where high-altitude clouds are responding to GCR variations and to understand

229 the possible contributing factors determining their susceptivity, although high-
230 resolution analyses might fail to capture the responses of the clouds that are not
231 stationed and randomly advected after being formed or those whose locations
232 are under the influence of other interannual variations such as the El Niño–
233 Southern Oscillation. Significant positive correlations were found in tropical
234 regions; however, they were concentrated over land and nearby oceans,
235 suggesting the importance of any of or all the following factors: (1) the presence
236 of relatively deeper convections compared with oceans, (2) the abundance of
237 continental aerosol precursors for ions to produce aerosols, and (3) a more
238 pronounced diurnal cycle over lands (see below). Most notable correlations were
239 found in August around West and Central Africa, India and Bangladesh, the
240 northwest coast of South America, and the proximate oceans, with a lag of 0–1
241 years (Fig 1a–b). The correlations around eastern India and Bangladesh suggest
242 that the sea breezes blowing toward elevated mountains may also contribute to
243 creating an environment in which cloud formations become sensitive to GCRs.
244 They uplift a substantial amount of water vapor and aerosol precursors to the
245 upper troposphere, similar to deep convection. The signals around the northwest
246 coast of South America in January (Fig 2a–b) and in the southern Brazil in
247 February (see Fig S11) may also be related to the same mechanism. Even though

248 convective cloud formation is active over Brazil in austral summer, the
249 correlations were not significant except for the areas facing oceans, thus
250 suggesting the importance of marine aerosol precursors for the impact of ions.
251 The more pronounced impact in August, compared with January, can be
252 associated with the relatively low pressure around the convective areas in August
253 (Fig 4e, also see Fig S12), which provides ideal conditions for supplying water
254 vapor and aerosol precursors to the upper troposphere. In other words, the
255 overlap of the Intertropical Convergence Zone (ITCZ) with the continental areas
256 could be the key to strengthening the GCR-cloud connection. The significant
257 northward excursion of ITCZ from the geomagnetic equator in August also
258 contributes in terms of the magnitude of the variability in ion production rate. As
259 also mentioned in the Results section, the variability of the abundance of GCR-
260 induced ions is greater at higher latitudes, especially at high altitudes (see Fig
261 S12b of [37]); thus, the excursion of ITCZ significantly increases the encounters
262 between ions and aerosol precursors. The lower pressure in August also
263 contributes to the higher GCR flux in the troposphere due to the reduced
264 barometric effect [48,49], although the associated enhancement is only a few
265 percent. The more significant impact in August may also be related to the
266 seasonal variability in the emission of organic compounds from biogenic activities,

267 the precursory materials for the aerosol formation [43,50]. For example, the flux
268 of dimethyl sulfide is maximum in the northern hemisphere from July to
269 September and is especially enhanced around the north part of the Indian Ocean,
270 near the continental areas [51].

271 Although the climatological condition is similar for July and August, the
272 correlations between high clouds and GCRs are significantly different. The impact
273 in July is sparse and not notable for a lag of 0-1 years (see Fig S13a–b), while
274 correlations become pronounced around the Indonesian maritime continent for a
275 lag of 2–3 years (see below). The possible explanation for the relatively weaker
276 response in July may be related to the influence of the updrafted preexisting
277 aerosols masking the impact of GCRs. For example, the abundance of mineral
278 dust in northern Africa is maximum in June and starts to decrease in July [52]. It
279 has also been reported that the aerosol optical depth in northern India is
280 maximum in May and that it starts to decrease in July [53]. Further examinations
281 are, however, needed to confirm the impact of preexisting aerosols.

282 The tendency of the decreased pressure peaking with a lag of 1 year around
283 tropical zones except for the Pacific region (Fig 4a–c) can be related to the
284 activated formation of deep convective clouds, and it may be causing positive
285 feedback to the promotion of cloud activity by the GCRs. It has been suggested

286 that the enhancement of aerosols may strengthen deep convection by increasing
287 freezing water droplets and releasing latent heat [54]. The synchronized
288 activation of convections over land in tropical regions may result in a tendency of
289 decreased pressure around the area. Please note that while the correlations
290 between clouds and GCRs were observed most significantly at the high altitudes,
291 the process behind the intensification of deep convective cloud activities may also
292 act at the middle layer of deep convective clouds. As mentioned in the
293 Introduction, deep convection may transport the newly-formed cloud
294 condensation nuclei to the lower altitudes.

295 The pressure decrease is more prominent over oceans and is significantly
296 weaker over land (Fig 4b), and this might be related to the more pronounced
297 diurnal cycle over land [55], which may mask the signals of the transient pressure
298 decreases in monthly averaged data. However, the diurnal cycle over land is
299 probably playing an essential role in sustaining convective activity and supplying
300 aerosol precursors to the upper troposphere, even under enhanced cloud
301 formation. In fact, the precipitation pattern indicates increased precipitation
302 around the areas where high-altitude clouds are increased (see Fig S14),
303 supporting this tendency. Increased precipitation might also contribute to
304 removing preexisting aerosols from the atmosphere.

The changed pressure gradient may then affect atmospheric circulation (see Fig S10), allowing the change in the SST gradient over the Pacific Ocean (Fig 3a–e). The reduced formation of high-altitude clouds over the western Pacific (Fig 1a–b) can be associated to the westward relocation of deep convections around the area. Low-altitude clouds, instead, are likely increased around the western Pacific (see FigS15g–h), consistent with the previously found correlation between GCRs and low-altitude clouds in this region [34]. It is worth noting that this is a region of typhoon generation. While more high-altitude clouds are expected for the higher GCR flux around the areas where hurricanes are generated, less typhoon activity is predicted for the higher GCR flux.

The westward extension of trade wind over the Pacific eventually warms the ocean around Indonesian maritime continent and off the northeast coast of Australia, and this warmth is maximized with a lag of 2–3 years (Fig 3c–d). The enhancement of high-altitude clouds around the area with a lag of 2–3 years can be related to this increased SST. The correlation between the GCRs and the SST in the northern part of the Pacific Ocean with a lag of ~2 years suggests that the altered atmospheric circulation pattern may also eventually contribute to modulating the Pacific Decadal Oscillation, although the mechanism behind the connection to the Pacific Decadal Oscillation remains unknown and thus needs

further examination.

The responses of atmospheric circulation and SST to the GCR cycles are similar to those suggested as a response to TSI cycles in previous studies; however, there are two notable differences. The first is the overall delay in the signals in the case compared with TSI (Fig 3h–l and Fig 4g–j), consistent with the ~1-year delay of GCRs to TSI, and the second is the warmth of the eastern Indian Ocean as an immediate response to TSI (Fig 3h and 3n). This feature, however, contradicts the weakening of the easterly wind in the western Pacific and the cooling tendency around the region suggested for the TSI maxima, as seen for the lag of 2–4 years (Fig 3j–l). Instead, it is more likely that this signal is related to the positive response to GCR with a lag of ~4 years (Fig 3e), which is a remnant of the impact around the Indonesian maritime continent (Fig 3d). In other words, a pseudo negative response with a five-year lag is expected for the case of TSI due to the delay of GCR to TSI by ~1 year. However, five years are nearly 180 degrees of a decadal solar cycle, thus resulting in the apparent immediate positive response to TSI (Fig 3h).

The possible solar influence pathway on climate systems through the variation of GCRs can be summarized as follows. First, GCRs impact the deep convective cloud activities in the tropics, primarily over the land areas, resulting in a decrease

in pressure around the area, possibly giving positive feedback to cloud formation. Second, the reduced pressure changes atmospheric circulation and the SST pattern over the Pacific. Finally, the altered SST pattern activates the high-altitude cloud formation around the Indonesian maritime continent. Note that although the suggested characteristic response of clouds to GCRs seems to support the existence of GCR's impact through the formation of aerosols, it is possible that they also affect clouds by the other paths, such as promoting the collisions between aerosols and cloud droplets [28–30]. Further investigations are needed to quantitatively understand the mechanisms of GCR's impact on the deep convective cloud activities, possibly through multiple paths.

It is noteworthy that no correlation was observed around the eastern Pacific region, where the El Niño–Southern Oscillation is most prominent. It was, however, found that the areas showing response to GCRs include the regions where periodic behaviors are often observed in SST, such as El Niño Modoki, the Indian Ocean Dipole, and the Pacific Decadal Oscillation. It is, therefore, possible that the GCRs may enhance the variability of the decadal component in such periodic behaviors, but with a few years of time lag. Further investigations on the proposed impacts of GCRs on cloud activity and atmospheric circulation may shed light on the variability or the phase changes of the decadal-scale

components in such unresolved oceanic variations.

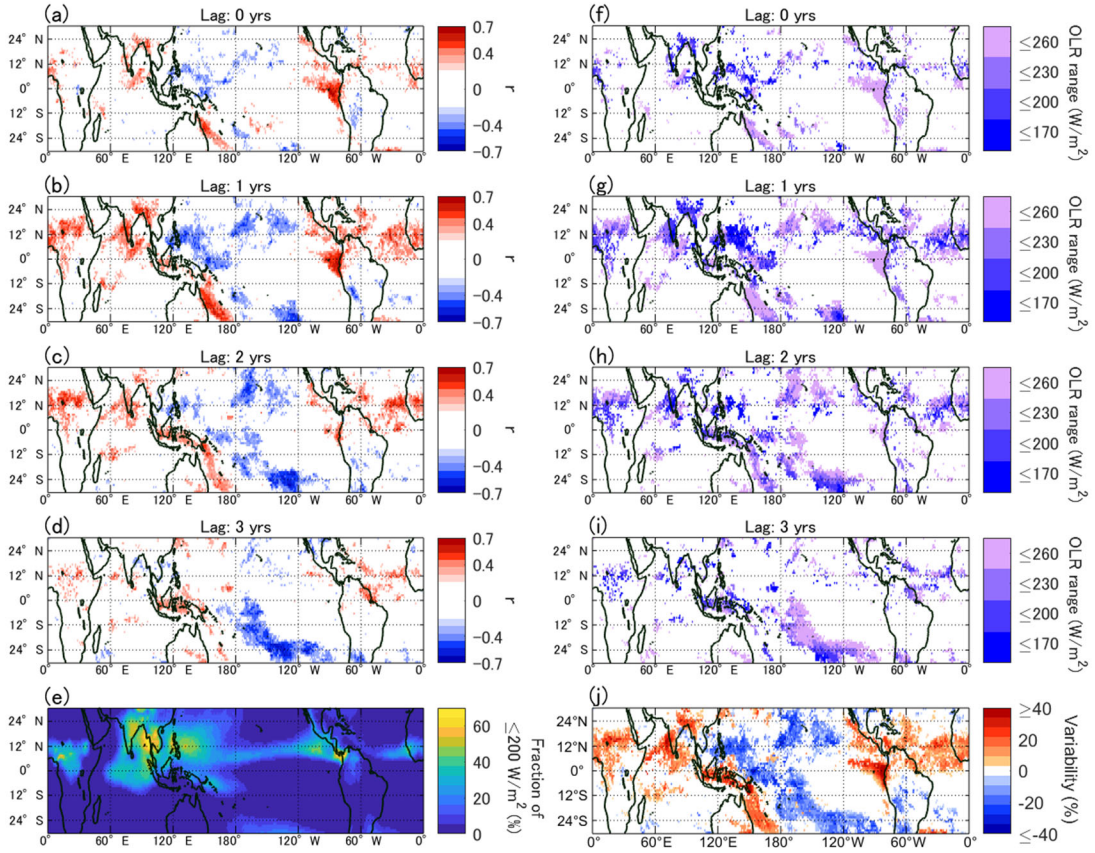

Figure 1. (a–d) Correlation coefficient r ($p \leq 0.05$) between the existence ratio of high-altitude clouds and GCRs in August for a time lag of 0–3 years. (e) Fraction of the days OLR is ≤ 200 W/m^2 in August. (f–i) OLR ranges that yielded the maximum correlation coefficients in (a–d). (j) Maximum variability of the existence ratio of high-altitude clouds over the GCR cycles.

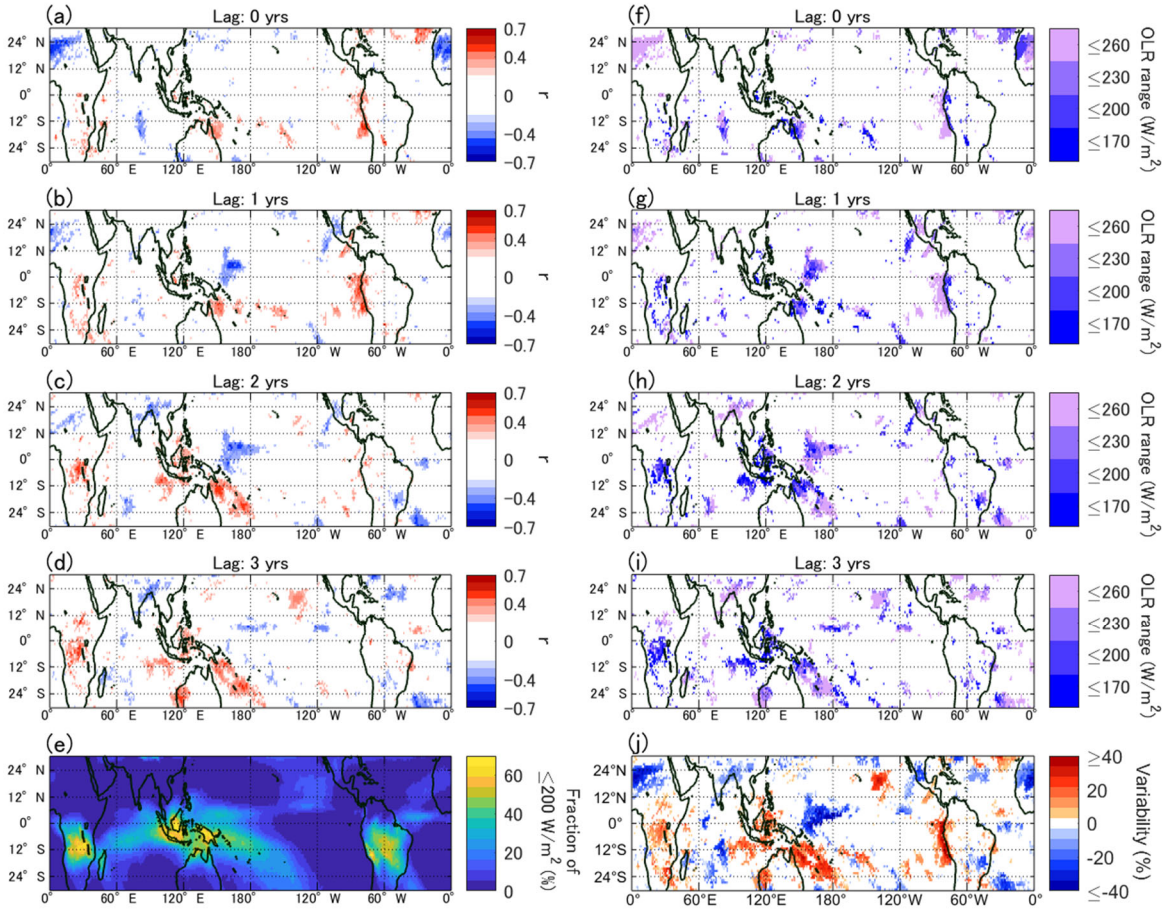

371

372 Figure 2. Same as Fig. 1 but for January.

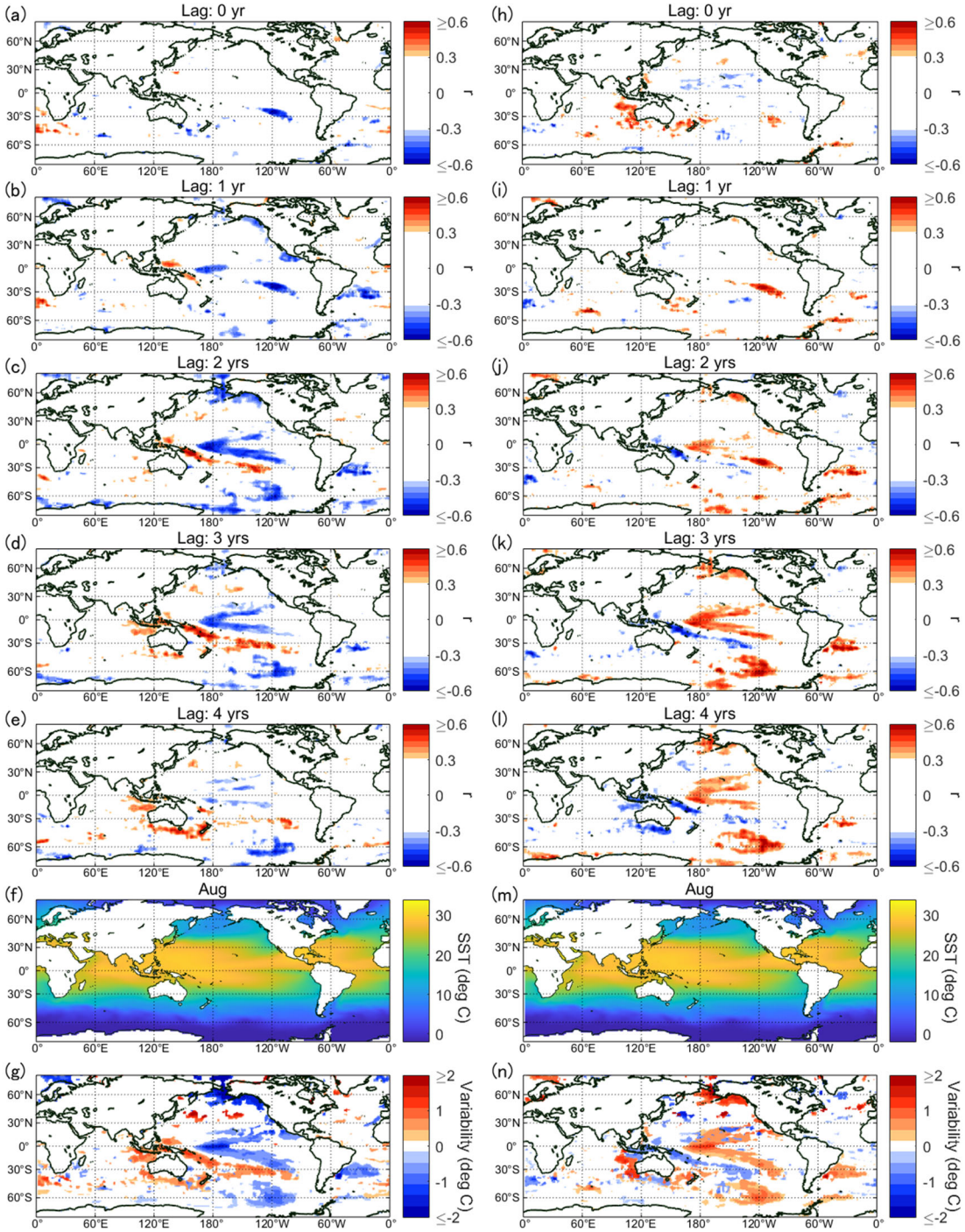

Figure 3. (a–e) Correlation coefficient r ($p \leq 0.05$) between GCRs and SST in August for a lag of 0–4 years. (f) Monthly mean SST for August. (g) Maximum variability of SST over the GCR cycles. (h–n) Same as (a–g) but for TSI.

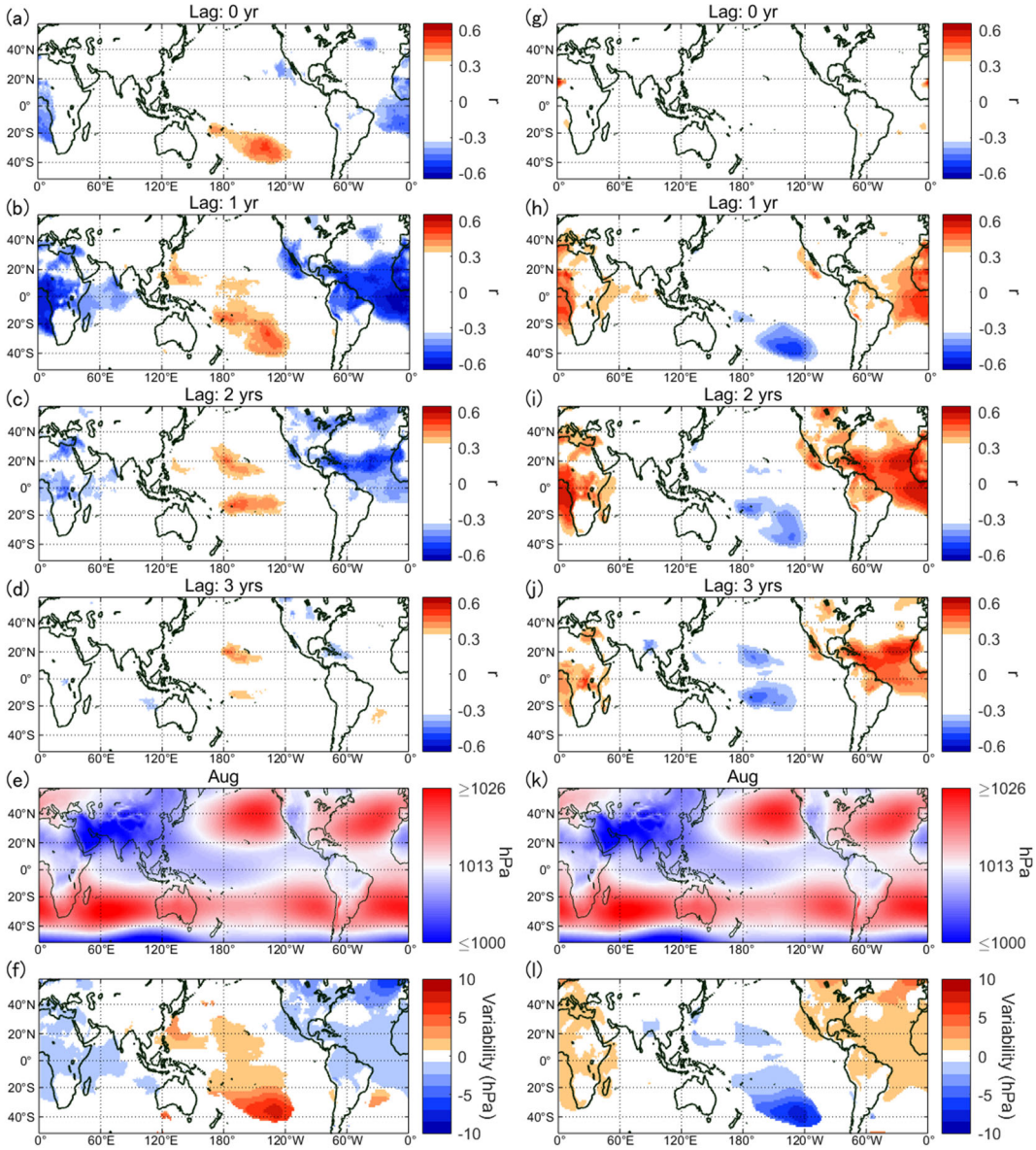

Figure 4. (a–d) Correlation coefficient r ($p \leq 0.05$) between surface pressure and GCRs in August for a lag of 0–3 years. (e) Monthly mean pressure reduced to the mean sea level for August. (f) Maximum variability of surface pressure over the GCR cycles. (g-l) Same as (a–f) but for TSI.

Methods

To examine the response of high-altitude clouds to GCR decadal cycles, we utilized a daily record of OLR [56] with 1° × 1° resolution for Jan/1979–Dec/2021. OLR reflects the existence of high-altitude clouds, although only for low-latitude regions. We calculated the fraction of the days OLR is equal to or lower than a threshold value for each month. We produced four time series for each grid with a threshold value: 170 W/m^2, 200 W/m^2, 230 W/m^2, and 260 W/m^2, respectively. They were then compared with the GCR variation to derive the Spearman's correlation coefficient. The maximum correlation coefficient among the four cases and the corresponding threshold were displayed on the maps. In the tropical regions, if the maximum correlation was obtained with the threshold of 200 W/m2, it implies that high-altitude clouds (cloud top pressure ≤ ~440 mb) are most sensitively responding to GCRs. On the other hand, if the maximum correlation was obtained with 230 W/m2, it suggests that adding mid-altitude clouds (~440 mb < cloud top pressure ≤ 680 mb) improves the correlation.

The response of clouds to GCR may accompany some time lags; therefore, correlations were examined for lags between 0 and 3 years. To estimate the correlation coefficient at a lag of zero years, the correlation coefficients for −2 years (GCRs lag cloud variation with two years) to 0 years (no time lag) were

403 calculated, and only the cases correlation was maximized at 0 years were
404 displayed. For the zero-year lag, the cloud data were compared with the monthly
405 mean GCR flux and with the yearly mean for a lag of 1 year or longer. For the
406 grids where the high-altitude clouds were absent or 100% for more than fifty
407 percent of the analyzed years, we excluded them from the analyses. With the lag
408 and threshold that yielded the maximum correlation coefficient, we estimated,
409 based on the regression line, the maximum variability of high-altitude clouds over
410 the GCR cycles, i.e., the variability for 1987–1990 when GCR variation was at its
411 maximum. For the GCR variation, the neutron monitor data for Jan/1953–
412 Nov/2006 obtained at the Climax station (http://cr0.izmiran.ru/clmx/main.htm) and
413 those for Apr/1964–Dec/2021 obtained at the Oulu station
414 (http://cr0.izmiran.ru/oulu/main.htm) were used. The daily data were normalized
415 and averaged to obtain the monthly means. Prior to the analyses, the long-term
416 trends were subtracted from the cloud and GCR data to concentrate on the
417 decadal-scale variations.

418 We also analyzed the ISCCP-HGM series provided by the International Satellite
419 Cloud Climatology Project [57] to validate the response of OLR to GCRs. We
420 used the monthly data of high (≤ 440 mb) and low (> 680 mb) cloud fractions for
421 July/1983–June/2017.

For the examination of the response of SST, we used the NOAA Optimum Interpolation SST V2 data provided by NOAA/OAR/ESRL PSL [58]. We used the 1-degree grid data for Dec/1981–Dec/2021. We also used the Niño 4 index [59] and the NCEI Pacific Decadal Oscillation index [60]. To analyze the response of surface pressure, zonal wind, and meridional wind, we used the JRA-55 (Japanese 55-year Reanalysis) data of monthly mean pressure reduced to mean sea level with 1.25° × 1.25° resolution [61]. We only used data from 1979 when the observational data was substantial and the reliability was high [62]. For the precipitation analysis, we used CMAP monthly mean precipitation data with 2.5° × 2.5° resolution [63].

To examine the responses of SST and atmospheric data to TSI, the NOAA Climate Data Record of TSI [64] was used. As an index of solar UV, NOAA adjusted the solar radio flux at 10.7cm (https://lasp.colorado.edu/lisird/data/noaa_radio_flux/) were combined with the Penticton radio flux data for May/2018 to present (https://lasp.colorado.edu/lisird/data/penticton_radio_flux/).

Note that the data from Jun/1991 to May/1993 were excluded from the analyses so that the possible impacts from the eruption of Mt. Pinatubo in 1991 are eliminated.

Acknowledgments

We thank S. Masuda, H. Yamada, Y. Yamashiki, K. Munakata, for discussions. This work was supported by JSPS KAKENHI grand number 15H05816 and the research scholarship provided to Musashino Art University by H. Suzuki. H.M. thanks Okinawa Institute of Science and Technology for hosting her sabbatical visit.

References

1. Gray LJ, Beer J, Geller M, Haigh JD, Lockwood M, Matthes K, et al. Solar influences on climate. Rev Geophys. 2010; 48: RG4001.

2. Kodera K, Kuroda Y. Dynamical response to the solar cycle. Journal of Geophysical Research. 2002; 107: 4749.

3. Matthes K, Kuroda Y, Kodera K, Langematz U. Transfer of the solar signal from the stratosphere to the troposphere: Northern winter. Journal of

Geophysical Research. 2006; 111: D06108.

4. Meehl GA, Arblaster JM, Branstator G, van Loon H. A coupled air–sea response mechanism to solar forcing in the Pacific region. Journal of Climate. 2008; 21: 2883–2897.

5. Misios S, Gray LJ, Knudsen MF, Karoff C, Schmidt H, Haiigh JD. Slowdown of the Walker circulation at Solar Cycle Maximum. Proceedings of the National Academy of Sciences of the United States of America. 2019; 116: 7186–7191.

6. Svensmark H, Friis-Christensen E. Variation of cosmic ray flux and global cloud coverage—A missing link in solar-climate relationships. Journal of Atmospheric and Solar-Terrestrial Physics. 1997; 59: 1225–1232.

7. Carslaw KS, Harrison RG, Kirkby J. Cosmic rays, clouds, and climate. Science. 2002; 298: 1732–1737.

8. Bond GC, Kromer B, Beer J, Muscheler R, Evans MN, Showers W, et al. Persistent solar influence on North Atlantic climate during the Holocene.

Science. 2001; 294: 2130–2136.

9. Obrochta SP, Miyahara H, Yokoyama Y, Crowley TJ. A re-examination of evidence for the North Atlantic “1500-year cycle” at Site 609. Quaternary Science Reviews. 2012; 55: 23–33.

10. Neff U, Burns SJ, Mingini A, Mudelsee M, Fleitmann D, Matter A. Strong coherence between solar variability and the monsoon in Oman between 9 and 6 kyr ago. Nature. 2001; 411: 290–293.

11. Wang Y, Cheng H, Edwards RL, He Y, Kong X, An Z, et al. The Holocene Asian monsoon: Links to solar changes and North Atlantic climate. Science. 2005; 308: 854–857.

12. Miyahara H, Yokoyama Y, Masuda K. Possible link between multi-decadal climate cycles and periodic reversals of solar magnetic field polarity. Earth and Planetary Science Letters. 2008; 272: 290–295.

13. Yamaguchi YT, Yokoyama Y, Miyahara H, Sho K, Nakatsuka T. Synchronized

Northern Hemisphere climate change and solar magnetic cycles during the Maunder Minimum. Proceedings of the National Academy of Sciences of the United States of America. 2010; 107: 20697–20702.

14. Domingo V, Ermolli J, Fox P, Fröhlich C, Haberrerter M, Krivova N. Solar surface magnetism and irradiance on time scales from days to the 11-year cycle. Space Science Reviews. 2009; 145: 337–380.

15. Jokipii JR, Thomas B. Effects of drift on the transport of cosmic rays. IV. Modulation by a wavy interplanetary current sheet. The Astrophysical Journal. 1981; 243: 1115–1122.

16. Forbush S. On cosmic-ray effects associated with magnetic storms. Journal of Geophysical Research. 1938; 43: 203–218.

17. Usoskin IG, Mursula K, Kananen H, Kovaltsov GA. Dependence of cosmic rays on solar activity for odd and even solar cycles. Advances in Space Research. 2001; 27: 571–576.

18. Koldobskiy SA, Kähkönen R, Hofer B, Krivova NA, Kovaltsov GA, Usoskin I. Time lag between cosmic-ray and solar variability: Sunspot Numbers numbers and open solar magnetic flux. Solar Physics. 2022; 297: 38.

19. Kodera K. Solar cycle modulation of the North Atlantic Oscillation: Implication in the spatial structure of the NAO. Geophysical Research Letters. 2002; 29: 59–51.

20. Gray LJ, Woollings TJ, Andrews M, Knight J. Eleven-year solar cycle signal in the NAO and Atlantic/European blocking. Quarterly Journal of the Royal Meteorological Society. 2016; 142: 1890–1903.

21. Kuroda Y, Kodera K, Yoshida K, Yukimoto S, Gray L. Influence of the solar cycle on the North Atlantic oscillation. Journal of Geophysical Research. Atmospheres. 2022; 127: e2021.

22. Gleisner H, Thejll P. Patterns of tropospheric response to solar variability. Geophysical Research Letters. 2003; 30: 1711.

23. van Loon H, Meehl GA, Arblaster JM. A decadal solar effect in the tropics in July–August. Journal of Atmospheric and Solar-Terrestrial Physics. 2004; 66: 1767–1778.

24. White WB. Response of tropical global ocean temperature to the Sun's quasi-decadal UV radiative forcing of the stratosphere. Journal of Geophysical Research. 2006; 111: C09020.

25. Dickinson RE. Solar variability and the lower atmosphere. Bulletin of the American Meteorological Society. 1975; 56: 1240–1248.

26. Kirkby J, Curtius J, Almeida J, dunne E, Duplissy J, Ehrhart S, et al. Role of sulphuric acid, ammonia and galactic cosmic rays in atmospheric aerosol nucleation. Nature. 2011; 476: 429–433.

27. Svensmark H, Enghoff MB, Pedersen JOP. Response of cloud condensation nuclei (> 50 nm) to changes in ion-nucleation. Physics Letters A. 2013; 377: 2343–2347.

555 28. Tinsley BA. Influence of solar wind on the global electric circuit, and inferred
556 effects on cloud microphysics, temperature, and dynamics in the troposphere.
557 Space Science Reviews. 2000; 94: 231–258.
558
559 29. Zhou L, Tinsley BA, Plemmons A. Scavenging in weakly electrified saturated
560 and subsaturated clouds, treating aerosol particles and droplets as
561 conducting spheres. Journal of Geophysical Research. 2009; 114: D18201.
562
563 30. Tinsley BA. Uncertainties in evaluating global electric circuit interactions with
564 atmospheric clouds and aerosols, and consequences for radiation and
565 dynamics. Journal of Geophysical Research: Atmospheres. 2022; 127:
566 e2021JD035954.
567
568
569 31. Tinsley BA, Deen GW. Apparent tropospheric response to MeV-GeV particle
570 flux variations: A connection via electrofreezing of supercooled water in high-
571 level clouds? Journal of Geophysical Research. 1991; 96: 22283–22296.
572
573 32. Yu F, Turco RP. From molecular clusters to nanoparticles: Role of ambient
574 ionization in tropospheric aerosol formation. Journal of Geophysical

575 Research: Atmospheres. 2001; 106: 4797–4814.

576

577 33. Yu F. Altitude variations of cosmic ray induced production of aerosols:
578 Implications for global cloudiness and climate. Journal of Geophysical
579 Research. 2002; 107: A7.

580

581 34. Marsh N, Svensmark H. Galactic cosmic ray and el Niño–Southern Oscillation
582 trends in International Satellite Cloud Climatology Project D2 low-cloud
583 properties. Journal of Geophysical Research: Atmospheres. 2003; 108: 4195.

584

585 35. Kazil J, Lovejoy ER, Barth MC, O'Brien K. Aerosol nucleation over oceans and
586 the role of galactic cosmic rays. Atmospheric Chemistry and Physics. 2006;
587 6: 4905–4924.

588

589 36. Yu F, Wang Z, Luo G, Turco R. Ion-mediated nucleation as an important global
590 source of tropospheric aerosols. Atmospheric Chemistry and Physics. 2008;
591 8: 2537–2554.

592

593 37. Dunne EM, Gordon H, Kürten A, Almeida J, Duplissy J, Williamson C, et al.

Global atmospheric particle formation from CERN CLOUD measurements. Science. 2016; 354: 1119–1124.

38. Ney ER. Cosmic radiation and weather. Nature. 1959; 183: 451–452.

39. Ermakov VI, Bazilevskaya GA, Pokrevsky PE, Stozhkov YI. Ion balance equation in the atmosphere. Journal of Geophysical Research: Atmospheres. 1997; 102: 23413–23419.

40. Usoskin IG, Gladysheva OG, Kovaltsov GA. Cosmic ray-induced ionization in the atmosphere: Spatial and temporal changes. Journal of Atmospheric and Solar-Terrestrial Physics. 2004; 66: 1791–1796.

41. Twohy CH, Clement CF, Gandrud BW, Weinheimer AJ, Campos TL, Baumgardner D, et al. Deep convection as a source of new particles in the midlatitude upper troposphere. Journal of Geophysical Research: Atmospheres. 2002; 107: 4560.

42. Williamson CJ, Kupc A, Axisa D, Bilsback KR, Bui TP, Campuzano-Jost P, et

al. A large source of cloud condensation nuclei from new particle formation in the tropics. Nature. 2019; 574: 399–403.

43. Almeida J, Schobesberger S, Kürten A, Ortega IK, Kupiainen-Määttä, Praplan AP, et al. Molecular understanding of sulphuric acid–amine particle nucleation in the atmosphere. Nature. 2013; 502: 359–363.

44. Koffi B, Schulz M, Bréon F-M, Dentener F, Steensen BM, Griesfeller J, et al. Evaluation of the aerosol vertical distribution in global aerosol models through comparison against CALIOP measurements: AeroCom phase II results. Journal of Geophysical Research: Atmospheres. 2016; 121: 7254–7283.

45. Evan AT, Heidinger AK, Vimont DJ. Arguments against a physical long-term trend in global ISCCP cloud amounts. Geophys Res Lett. 2007; 34: L04701.

46. Ashok K, Behera SK, Rao SA, Weng H, Yamagata T. El Niño Modoki and its possible teleconnection. Journal of Geophysical Research. 2007; 12: C11007.

47. Mantua MK, Hare SR, Zhang Y, Wallace JM, Francis RC. A Pacific interdecadal climate oscillation with impacts on salmon production. Bulletin of

633 the American Meteorological Society. 1997; 78: 1069–1080.

634

635 48. Myssowsky L, Tuwim L. Unregelmassige Intensitätsschwankungen der
636 Hohenstrahlung in geringer Seehohe. Zeitschrift für Physik A – Hadrons and
637 Nuclei, 1926; 39: 146–150.
638 49. De Mendonça RRS, Raulin J-P, Echer E, Makhmutov VS, Fernandez G.
639 Analysis of atmospheric pressure and temperature effects on cosmic ray
640 measurements. Journal of Geophysical Research: Space Physics. 2013; 118:
641 1403–1409.

642

643 50. Kirkby J. Cosmic rays and climate. Surveys in Geophysics. 2007; 28: 333–
644 375.

645

646 51. Land PE, Shutler JD, Bell TG, Yang M. Exploiting satellite Earth observation
647 to quantify current global oceanic DMS flux and its future climate sensitivity.
648 Journal of Geophysical Research: Oceans. 2014; 119: 7725–7740.

649

650 52. Vandenbussche S, Callewaert S, Schepanski K, De Mazière M. North African
651 mineral dust sources: New insights from a combined analysis based on 3D

652 dust aerosol distributions, surface winds and ancillary soil parameters.
653 Atmospheric Chemistry and Physics. 2020; 20: 15127–15146.
654
655 53. Gautam R, Hsu NC, Lau K-M. Premonsoon aerosol characterization and
656 radiative effects over the Indo-Gangetic Plains: Implications for regional
657 climate warming. Journal of Geophysical Research. 2010; 115: D17208.
658
659 54. Rosenfeld D, Lohmann U, Raga GB, O'Dowd CD, Kulmala M, Fuzzi S, et al.
660 Flood or drought: How do aerosols affect precipitation? Science. 2008; 321:
661 1309–1313.
662
663 55. Yang G-Y, Slingo J. The diurnal cycle in the tropics. Monthly Weather Review.
664 2001; 129: 784–801.
665
666 56. Lee HT and NOAA CDR Program. NOAA Climate Data Record (CDR) of Daily
667 Outgoing Longwave Radiation (OLR), Version 1.2. NOAA National Climatic
668 Data Center. 2001. doi:10.7289/V5SJ1HH2. (Date of access: 15/01/2022)
669
670 57. Rossow WB, Walker A, Golea V, Knapp KR, Young A, Inamdar A, et al.

671 International Satellite Cloud Climatology Project Climate Data Record, H-
672 Series HGM NOAA National Centers for Environmental Information. 2016.
673 doi:10.7289/V5QZ281S.
674
675 58. Reynolds RW, Rayner NA, Smith TM, Stokes DC, Wang W. An improved in
676 situ and satellite SST analysis for climate. Journal of Climate. 2002; 15: 1609–
677 1625.
678
679 59. Trenberth KE, Stepaniak DP. Indices of El Niño evolution. Journal of Climate.
680 2001; 14: 1697–1701.
681
682 60. Mantua NJ. The Pacific Decadal Oscillation and Climate Forecasting for North
683 America. In: Golnaraghi M, editor. Climate Risk Solutions. Seattle: University of
684 Washington; 1999. pp. 10–13.
685
686 61. Kobayashi S, Ota Y, Harada Y, Ebita A, Moriya M, Onoda H, et al. The JRA-
687 55 Reanalysis: General Specifications and Basic Characteristics. Journal of the
688 Meteorological Sciety of Japan. 2015; 93: 5–48.
689

690 62. Ebita A, Kobayashi S, Ota Y, Moriya M, Kumabe R, Onogi K, et al. The
691 Japanese 55-year Reanalysis “JRA-55”: An Interim Report. Sola. 2011; 7: 149–
692 152.
693
694 63. Huffman GJ, Adler RF, Arkin P, Chang A, Ferraro R, Gruber A, et al. The
695 Global Precipitation Climatology Project (GPCP) combined data set. Bull Amer
696 Meteor Soc. 1997;78: 5-20.
697
698 64. Coddington O, Lean JL, Lindholm D, Pilewskie P, Snow M, and NOAA CDR
699 Program. NOAA Climate Data Record (CDR) of Total Solar Irradiance (TSI),
700 NRLTSI version 2. N.O.A.A. National Centers for Environmental Information.
701 2015. doi:10.7289/V55B00C1.
702
703
704 **Data availability Statement**
705 The OLR data are available at https://www.ncei.noaa.gov/products/climate-
706 data-records/outgoing-longwave-radiation-daily. ISCCP-HGM series is available
707 at https://www.ncei.noaa.gov/products/international-satellite-cloud-climatology.
708 The Oulu and Climax neutron data are available at

709 http://cr0.izmiran.ru/clmx/main.htm and http://cr0.izmiran.ru/oulu/main.htm,
710 respectively. The NOAA OI SST V2 data are provided by NOAA/OAR/ESRL PSL
711 on their website: https://psl.noaa.gov/data/gridded/data.noaa.oisst.v2.html.
712 Japanese 55-year Reanalysis data are available at
713 https://rda.ucar.edu/datasets/ds628.1/. The ESRL/NOAA Niño 4 index is
714 available at https://psl.noaa.gov/data/correlation/nina4.data. The NCEI Pacific
715 Decadal Oscillation index is available at
716 https://www.ncei.noaa.gov/access/monitoring/pdo/. CMAP Precipitation data are
717 provided by NOAA/OAR/ESRL PSL on their website:
718 https://psl.noaa.gov/data/gridded/data.cmap.html. The NOAA Climate Data
719 Record of TSI are available at
720 https://www.ncei.noaa.gov/access/metadata/landing-
721 page/bin/iso?id=gov.noaa.ncdc:C00828. The data of NOAA adjusted solar radio
722 flux at 10.7cm is available at
723 https://lasp.colorado.edu/lisird/data/noaa_radio_flux/. The Penticton radio flux
724 data are available at https://lasp.colorado.edu/lisird/data/penticton_radio_flux/.
725